7B.1 Large eddy simulations of convective boundary layer during late afternoon transition

Clara Darbieu*(1), Fabienne Lohou(1), Fleur Couvreux (2), Marie Lothon(1), Pierre Durand(1), Françoise Guichard(2), Ned Patton(3)

(1) Université de Toulouse, Laboratoire d'Aérologie - CNRS UMR 5560, Toulouse, France
(2) CNRM/GAME, Météo France, Toulouse, France
(3) National Center for Atmospheric Research, Boulder, CO, USA

1. Introduction

The Boundary Layer Late Afternoon and Sunset Turbulence (BLLAST) campaign took place in France in June and July 2011 focusing on the evening collapse of the boundary layer (Lothon et al. (2012)). The BLLAST experiment gathered numerous different and complementary instruments to study the relatively unknown processes controlling the transition from a well-developed daytime atmospheric boundary layer (ABL) to a residual layer overlying a stably stratified surface layer. In an effort to guide the BLLAST instrument deployment and sampling strategies, the present numerical study aimed at answering basic questions such as : what is the start-time of the late afternoon transition (LAT)? Which atmospheric layers have to be experimentally investigated in priority ? To address these questions, two Large Eddy Simulations (LES) codes – the NCAR LES, and Meso-NH from Laboratoire d'Aérologie and CNRM/GAME were used to simulate a decaying convective boundary layer. Besides guiding the experimental design, this numerical study had two additional goals:
1/ To compare the two codes and their ability to simulate this delicate period during which the surface buoyancy flux is decreasing.
2/ To study the turbulence characteristics during this period. Results found in the literature are revisited and further analysed.
Sorbjan (1997) and Pino et al. (2004) studies show that universal linear profiles of buoyancy fluxes are not maintained in the LAT since they become ` S ´ shaped. In this study, we investigate the evolution of the buoyancy fluxes and quantify continuously in time the departure from linear profiles all along the afternoon. Niewstadt and Brost (1986) studied an idealized case of mixed-layer decay caused by a sharp cut of the surface sensible heat flux H. Sorbjan (1997) extended this study by simulating the decay of the TKE caused by a gradual decrease of a weak H. We investigate the impact of a stronger decrease of H on TKE decay at different heights in the ABL, based on a real case.

The case study and the models setup are presented in Section 2. After a comparison of the two simulations performed in Section 3.1, we investigate the validity of the normalization scalings during the LAT in Section 3.2. Finally, we study the temporal evolution of the profiles of buoyancy flux and turbulence, respectively in Section 3.3 and Section 3.4.

2. IHOP study case and models setup

Two Large Eddy Simulations (LES) codes the NCAR LES, and Meso-NH from Laboratoire d'Aérologie and CNRM/GAME were used to simulate a decaying convective boundary layer, without cloud. Both models are based on Navier-Stokes equations, including conservation laws for momentum, mass and the first law of thermodynamics. There is no large scale forcing, such as subsidence or advection, and no geostrophic wind. Moreover, there is no coupling with a surface model : surface sensible and latent heat fluxes are imposed.

These simulations were initialized with wind, temperature and humidity profiles (Figure 1), from the 14th of June data-set collected during the International H_2O Project (IHOP 2002) field experiment (Southern Great Plains/US, Weckwerth et al. (2004)). These initial conditions have been defined by Couvreux et al. (2005). The initial profiles of potential temperature θ (Figure 1a) and water vapor mixing ratio r_v (Figure 1b) represent a stable layer, with a mixing ratio of 12 g kg^{-1} at surface and 5 g kg^{-1} above 1000 m. The wind speed vertical profile (Figure 1c) reveals a strong shear above 1500 m. Sensible and latent heat fluxes reach respectively 200 W m^{-2} and 170 W m^{-2} at 1400 LT (Figure 1e and f).

The simulations last 14 hours, starting at 0700 LT and finishing at 2100 LT . The size of the simulated domain is 10 km in horizontal directions and 4.8 km in the vertical direction. Space increments are as follows : $\Delta x = \Delta y =$ 100 m, $\Delta z = 40$ m.

*corresponding author address: Clara Darbieu, Centre de Recherches Atmosphériques, 8 route de Lannemezan, 65300 Campistrous, France; *email*: darc@aero.obs-mip.fr

There are two main differences in the models setup :

* The time increment dt in NCAR is determined by a Courant-Freidrichs-Lewy (CFL, Courant, 1967) number of 0.5. dt varies between 2.2 s and 2.8 s in NCAR simulation whereas in Meso-NH, it remains constant and egal to 1 s.

* In NCAR, a null vertical velocity is imposed at the top of the ABL whereas in Meso-NH, the upper limit condition is nudged toward the initial conditions.

3. Results

Vertical profiles of potential temperature and humidity as well as sensible and latent heat fluxes, vertical wind profiles, vertical wind variance are presented. Then, results found in the literature are revisited and further analysed.

3.1 Comparison of NCAR and Meso-NH simulations

The intercomparison of the two simulations does not prove that the codes simulate correctly the afternoon transition, but it enables to verify whether both models give similar and coherent results for the LAT period.

The evolution of mean parameters and some turbulent moment vertical profiles are shown. For both simulations, profiles are averaged over 30 minutes and are plotted every hour, starting at 0900 LT.

3.1.1 Vertical profiles of potential temperature, humidity and the associated vertical turbulent fluxes

The evolution of the potential temperature profile in the simulation is depicted in Figure 2a: the potential temperature in the mixed layer steadily increases of about 10 K between 0700 LT and 2000 LT, and the mixed layer extends vertically, growing from 500 m to 2500 m. Both simulations give similar results, although Meso-NH ABL is slightly warmer.

Vertical profiles of the covariance between the vertical velocity and the potential temperature $\overline{w'\theta'}$ are shown in Figure 2b. They have the universal shape of flux in a convective boundary layer : positive at the surface, linearly decreasing with altitude, corresponding to a well mixed layer, until reversing in the entrainment zone, at

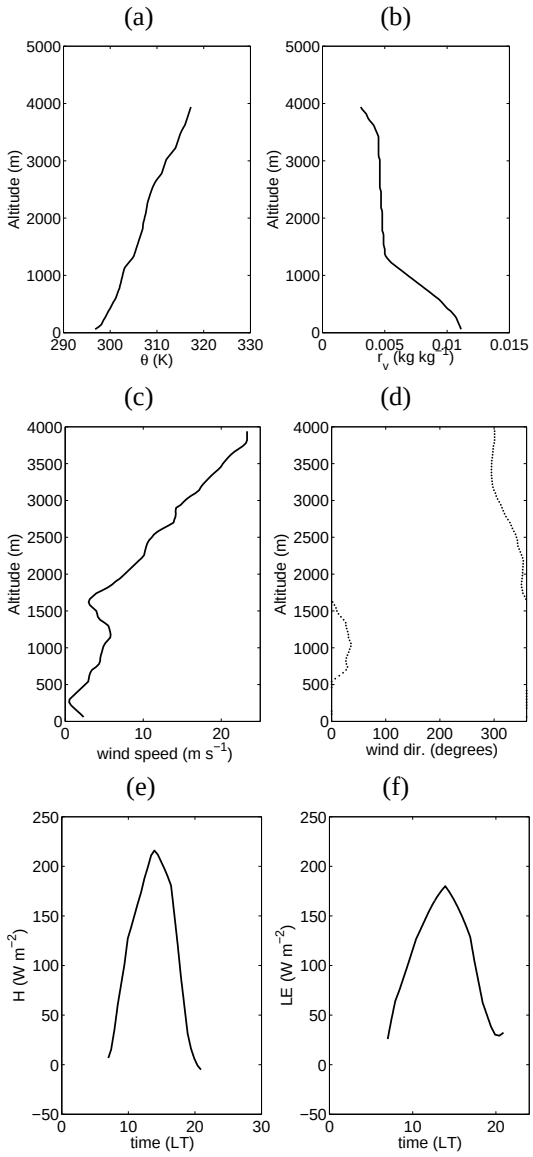

Figure 1: *Initial profiles of (a) potential temperature* θ*,(b) mixing ratio* r_v *,(c) wind speed, (d) wind direction and temporal evolution of surface (e) sensible and (f) latent heat fluxes, used in both simulations*

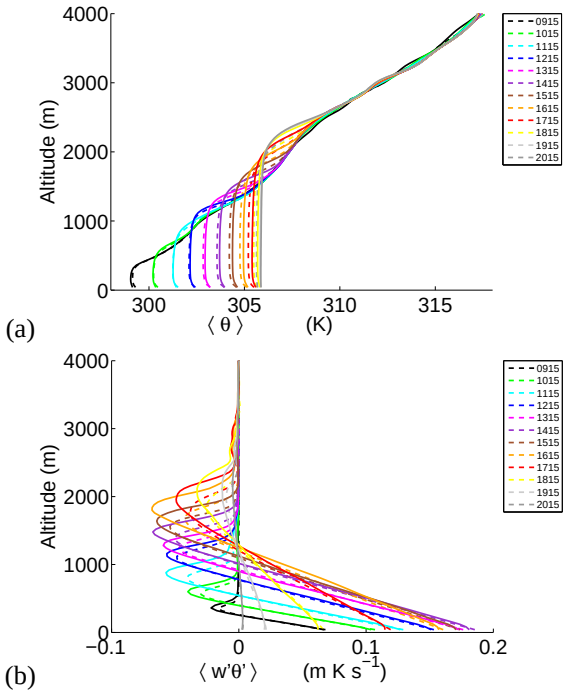

Figure 2: *Evolution of the vertical profile of (a) potential temperature $\overline{\theta}$ and (b) covariance $\overline{w'\theta'}$, every hour (color scale). NCAR (dotted lines), Meso-NH (continuous line)*

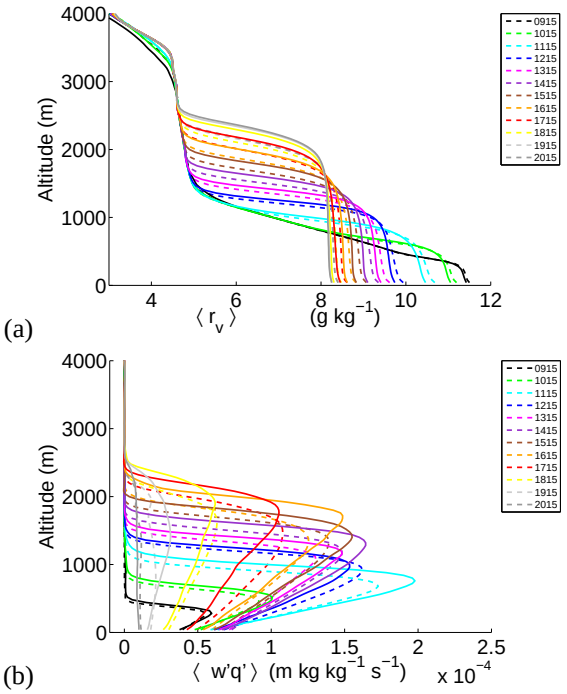

Figure 3: *Evolution of the (a) vertical profile of the water vapor mixing ratio r_v and (b) covariance $\overline{w'q'}$, every hour (color scale). NCAR (dotted lines), Meso-NH (continuous line)*

the top of the ABL, defined as z_i. One can note the higher values of $\overline{w'\theta'}$ at the top of the ABL in Meso-NH simulation.

The evolution of the profile of water vapor mixing ratio r_v and the covariance $\overline{w'q'}$ are shown respectively in Figure 3a and Figure 3b. Both simulations are quite similar, even though the humidity transfer from the ABL to the free atmosphere is higher in Meso-NH, inducing a slightly drier ABL in Meso-NH.

The entrainment ratio, defined as the magnitude of minus the buoyancy flux at z_i relative to the surface buoyancy flux, $\frac{-\overline{w'\theta'_v}_{zi}}{\overline{w'\theta'_v}_s}$, (where θ_v is the virtual potential temperature) is more important in Meso-NH than in NCAR simulation (not shown) : in Meso-NH, the entrainment ratio is of 0.4 instead of typical values of 0.25, which remains unexplained. So, the higher values of heat and humidity fluxes at the top of the ABL in Meso-NH are consistent with the larger values of entrainment in Meso-NH simulation. This likely explains the warmer and drier ABL in Meso-NH, by introducing dry air of the free troposphere.

3.1.2 *Vertical profiles of horizontal mean wind and variance of the vertical wind component*

For both simulations, horizontal mean wind is weak (about 5 m s^{-1} below 1500 m), then increases with altitude and reaches 20 m s^{-1} at 4000 m (Figure 4a). Vertical profiles of the variance of the vertical wind component are similar even though the variance is slightly stronger in Meso-NH (Figure 4b), especially in the afternoon, after 1615 LT.

To conclude, the two simulations give similar results concerning the time evolution of mean variables and vertical fluxes. The main differences come from larger values of entrainment in Meso-NH simulation, as well as a larger variance of the vertical wind component.

In the next section, we investigate the validity of the normalization scalings during the LAT. We will insist on the determination of the boundary layer height : is it still possible to define a convective boundary layer during this transition period ?

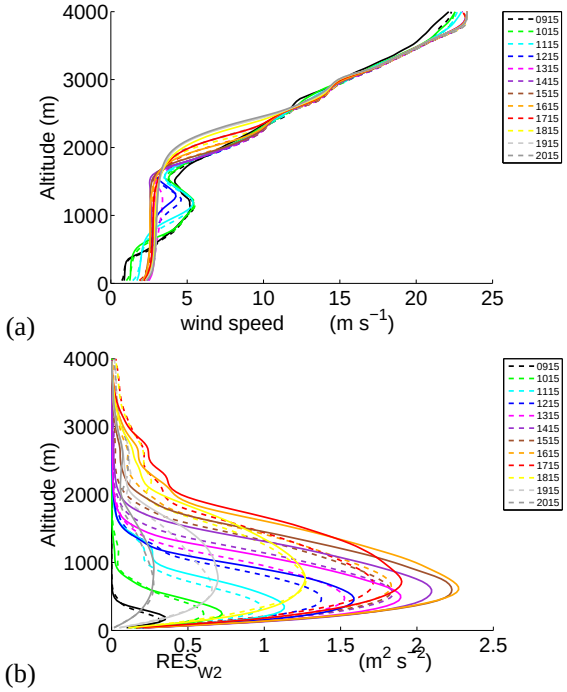

Figure 4: *Evolution of (a) vertical profiles of wind speed and (b) the resolved variance of the vertical wind component, every hour (color scale). NCAR (dotted lines), Meso-NH (continuous line)*

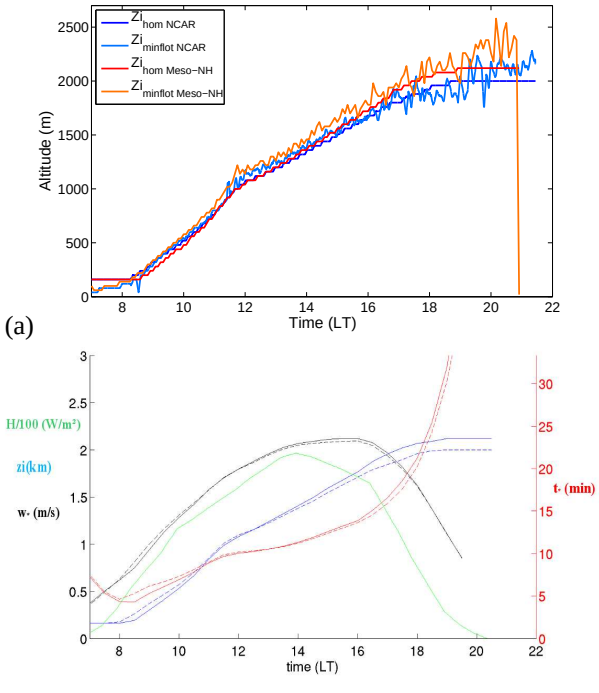

Figure 5: *(a) Temporal evolution of z_i, evaluated by two methods : by determining the altitude of the minimum buoyancy flux ($zi_{minflot}$) and by determining the thickness of the mixed layer (zi_{hom}).(b) Temporal evolution of w_* ($m\ s^{-1}$), t_*(min), zi_{hom} (km), $H/100$ ($W\ m^{-2}$) (b) in NCAR (dotted lines) and Meso-NH (continuous line)*

3.2 *Validity of normalization scales during the late afternoon transition*

Dimensionless turbulent characteristics are universal functions of the reduced altitude z/z_i. In order to represent these characteristics in their dimensionless form, different normalization scales defined by Deardorff (1972) are used.

$*$ The length scale, z_i, can be defined by several methods, which give different estimates (Figure 5a):

- From the vertical buoyancy profiles, z_i corresponds to the altitude of the minimum buoyancy flux.
- From the temperature vertical profiles, z_i can be defined as the altitude of the maximum temperature gradient. z_i can also be determined as the summit of the mixed layer, by using a threshold on the near-zero vertical gradient of potential temperature.

Figure 5a shows the evolution of the ABL height in the NCAR and Meso-NH simulations, from two methods. As observed on the flux profile (Figure 2b), the evolution of z_i is similar for both models, z_i being slightly upper in Meso-NH simulation, consistently with the larger entrainment flux discussed previously. However, after 1700 LT, z_i is not well defined by the minimum buoyancy flux. In our case, this method is relevant to determine z_i in a convective and developed ABL (i.e. in the middle of the day) whereas in the LAT period, although the tendency is kept, the very weak and fluctuating buoyancy profile makes the minimum flux determination very uncertain : some strong fluctuations of more than 400 m can be observed.

The method consisting in determining the altitude of the maximum temperature gradient (not shown) does not fit either in our case, since strong gradients are detected above 2500 m instead of the summital inversion.

However, the Meso-NH and NCAR simulations show that z_i is well defined by the height of the mixed layer, even during the transition period.

The boundary layer height is a very important parameter for normalization scales since it is included in the definition of the other scales, such as w_* or t_*.

$*$ The convective velocity scale w_* is defined as $(\beta \overline{w'\theta'}_s\ z_i)^{1/3}$, where $\beta = \frac{g}{T}$ is the buoyancy parameter and T is the mean temperature in the mixed layer.

$*$ The convective time scale $t_* = \frac{zi}{w_*}$.

$*$ The temperature scale $\theta_* = \frac{\overline{w'\theta'}_s}{w_*}$.

$*$ The humidity scale $q_* = \frac{\overline{w'q'_s}}{w_*}$.

For the following study, we define the convective scales t_{*0}, w_{*0} and θ_{*0} at the time when H is maximum (values are given in Table 1).

Figure 5b shows the temporal evolution of the convective scales t_* and w_*, z_i and H. w_* strongly increases until 1300 LT because of the increase of turbulence and convection. Then w_* stays approximately constant until 1600 LT and the convective mean time is about 15 minutes. After 1600 LT, z_i does not increase enough to compensate the decrease of the surface heat flux. Consequently, w_* decreases whereas t_* exponentially increases : at 1600 LT, 15 minutes are necessary for a thermal to go through the ABL whereas at 1900 LT, double time is required.
After 2000 LT, the surface heat flux becomes negative : these scales are not defined anymore.

As a conclusion, during the convective development of the ABL, the estimation of the length scale z_i is very coherent whatever the method used. On the contrary, during the LAT, the method leaning on the minimum value of the buoyancy flux should not be used because of the gradual loss of the universal shape of the vertical profile. Evaluating the top of the mixed layer using a threshold on the near-zero vertical gradient of potential temperature seems to be the most suitable method. Note that this method should remain appropriate later in the day, when a stabilizing layer is devoloping at the surface, with negative surface heat fluxes since this estimation of z_i corresponds to the top of the residual layer above and it may also be relevant for scaling. The other method leaning on the minimum value of the buoyancy flux should not be used because of the gradual loss of the universal shape of the vertical profile.

We are aware that the diminishing w_* and the exponential increase of t_* from 1600 LT might not be realistic in the late afternoon. Sorbjan (2007) shows that the conventional convective velocity scale is not adequate anymore during the decay phase. Besides, van Driel and Jonker (2011) raise the issue of defining new normalization scales in transitional situations, by prognosing the TKE from a rate equation that comprised dissipation and buoyancy production.

3.3 ` S ´ shape of buoyancy flux

Here, we consider the evolution of the shape of buoyancy flux profiles. We estimate whether universal linear profiles of buoyancy fluxes are maintained in the LAT or, as in Sorbjan (1997, 2007) and Pino et al. (2004), whether they become ` S ´ shaped.

Three vertical profiles of the dimensionless buoyancy fluxes (scaled by $w_*\theta_{v_*}$) are shown in Figure 6. At 1415 LT, the ABL is well developed, in a quasi stationary state : the profile of $\frac{\overline{w'\theta'_v}}{w_*\theta_{v*}}$ is linear with height. Then, as explained by Sorbjan (1997), in the afternoon, the flux vertical profiles become curved, due to the non-stationarity, especially near the surface. So, the maximum flux is not at the surface but in the lower part of the ABL, near surface. Figure 6 shows that at 1715 LT, the buoyancy flux looses its linearity, whereas the sensible heat flux is still important, about 131 W m^{-2}. At 1955 LT, the buoyancy flux is much more curved, but it corresponds to a very weak surface flux, about 6 W m^{-2}.

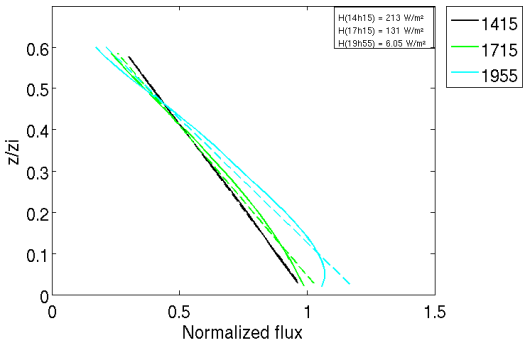

Figure 6: $\frac{\overline{w'\theta'_v}}{w_*\theta_{v*}}$ *vertical profiles at 1415 LT, 1715 LT and 1955 LT.*

To properly determine when the vertical profile of the buoyancy flux begins to be ` S ´ shaped, and to quantify continuously in time the curvature, the flux is fitted with a linear regression between the surface and $0.6z_i$ (Figure 7a), and the departure from linear profiles is evaluated by quantifying the area between the vertical profile and the linear regression (Figure 7b). From 1400 LT to 1600 LT, linear regressions correctly match the normalized profiles. The area between the flux and the regression is very small and constant. Between 1600 LT and 1900 LT, there is a slight increase of the area, associated with some fluctuations. After 1900 LT, the continuous increase of the area confirms the departure from linear profiles : profiles become ` S ´ shaped.

As a conclusion, the universal dimensionless buoyancy flux profiles are not linear anymore after 1700LT and become ` S ´ shaped. The strong fluctuations show how much it is difficult to estimate the curvature of the profiles as well as how sensitive is our estimation, which may be linked to the increase of t_*. Indeed, after 1700LT, the turbulent transfers are significantly different than during the convective period. The convective time scale seems not short enough to allow the ABL to correctly response to the rapid changes at surface.

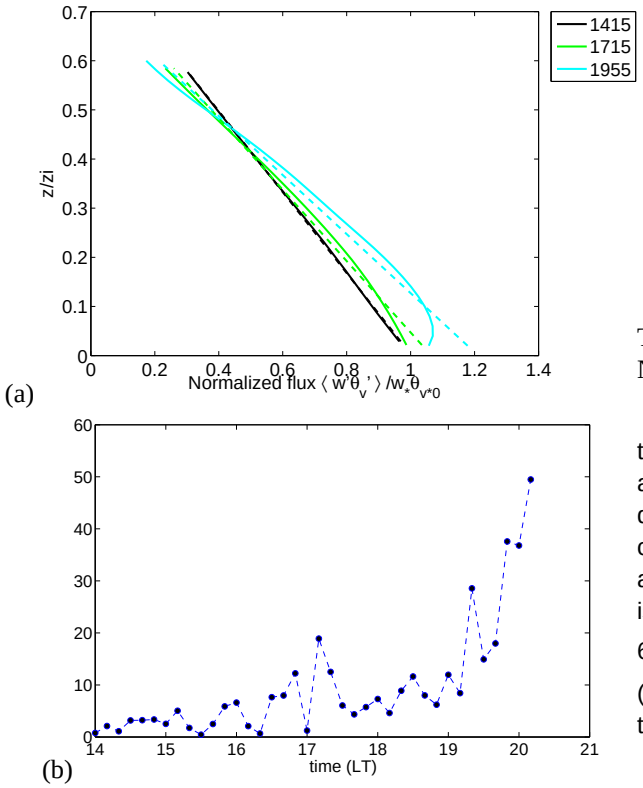

Figure 7: *(a)* $\frac{\overline{w'\theta'_v}}{w_*\theta_{v*}}$ *vertical profiles and their linear regressions at 1415 LT, 1715 LT and 1955 LT and (b) temporal evolution of the area between* $\frac{\overline{w'\theta'_v}}{w_*\theta_{v*}}$ *and the linear regression between 0 and 0.6* z_i .

3.4 Decay of TKE

3.4.1 Decay of the mean TKE in the ABL

Niewstadt and Brost (1986) studied an idealized case of mixed-layer decay caused by a sharp cut of the surface heat flux H. Sorbjan (1997) extended this study by stuying the decay of the TKE caused by a gradual decrease of H. According to his results, the evolution of the ABL is governed by two time scales: the external time scale τ_f, which controls the surface heat flux decrease, and the convective scale t_{*0}. τ_f is defined as the time lag between the maximum H flux and the zero flux. A quasi stationary regime is characterized by a negligible t_{*0}, relatively to τ_f. When t_{*0} and τ_f can reach similar values, the regime is not stationary anymore, and the convective scales become invalid (Sorbjan (1997)). Figure 8 represents the mean TKE in the ABL, normalized by w_{*0}^2, as a function of dimensionless time t/t_{*0}, for NCAR and Meso-NH simulations. According to Sorbjan, when the ratio of these two scales is small ($\tau_f/t_* << 1$), the decay of the normalized mean TKE is described by a power law following $(\frac{t}{t_*})^{-1.2}$. When the ratio is large ($\tau_f/t_* >> 1$), the TKE is quasi constant and follows $(\frac{t}{t_*})^0$. When $0 < \tau_f/t_* < \infty$, the functions describing the decay are confined between these two curves. Noticeable differences between our simulation and his are summarized in Table 1. The main difference is that $\tau_f = 1.4$ h in Sorbjan simulation, whereas $\tau_f = 6.41$ h in ours. Besides, the decay rate, defined as $\frac{\overline{w'\theta'_{max}}}{\tau_f}$ (K m h^{-2}) is four times smaller in Sorbjan simulation than in ours.

Characteristics	Sorbjan	IHOP
w_{*0} (ms^{-1})	0.613	2.0701
θ_{*0} (K)	0.0163	0.0966
$z_{i_{*0}}$ (m)	705	1300
t_{*0} (s)	1150	683
$\overline{w'\theta'}_{max}$ (Kms^{-1})	0.01	0.2
τ_f (h)	1.4	6.41
Decay rate = $\frac{\overline{w'\theta'}_{max}}{\tau_f}$ (Kmh^{-2})	25.71	112.32

Table 1: Characteristics comparison of Sorbjan and NCAR simulations

In our simulations, we also obtain a power law, in t^{-4} : the normalized TKE stays constant longer, then it decreases much faster. Besides, the very similar behavior of our two simulations gives consistency in our results

As a conclusion, this representation shows that the TKE decreases with time, and is a function of τ_f and t_{*0}. However, we have to keep in mind that the normalization scales w_{*0} and t_{*0} are defined when the surface heat flux is maximum, that is to say when the ABL is fully convective.

3.4.2 Evolution of the TKE at different heights in the ABL

Besides the decay of the mean TKE in the ABL, we are also interested in understanding how the TKE evolves in time at different heights in the ABL (Figure 9). Most of the energy remains in the lower ABL (up to 0.5zi), then decreases with height. One can notice that the TKE between 0 and 0.5 z_i evolves almost constantly from 1400 LT to 1700 LT. However, the TKE increases from 1400 LT at the top of the ABL, that is to say before the decay of TKE during the transition. At that time, z_i reaches the sheared layer above : the entrainment of momentum might explain this increase of TKE at the top of the ABL. Then, it seems that these high TKE values descend from the top of the boundary layer to the bottom, down to 0.4 z_i during the late afternoon, with entrainment gaining the upper hand over surface convective processes. Indeed,

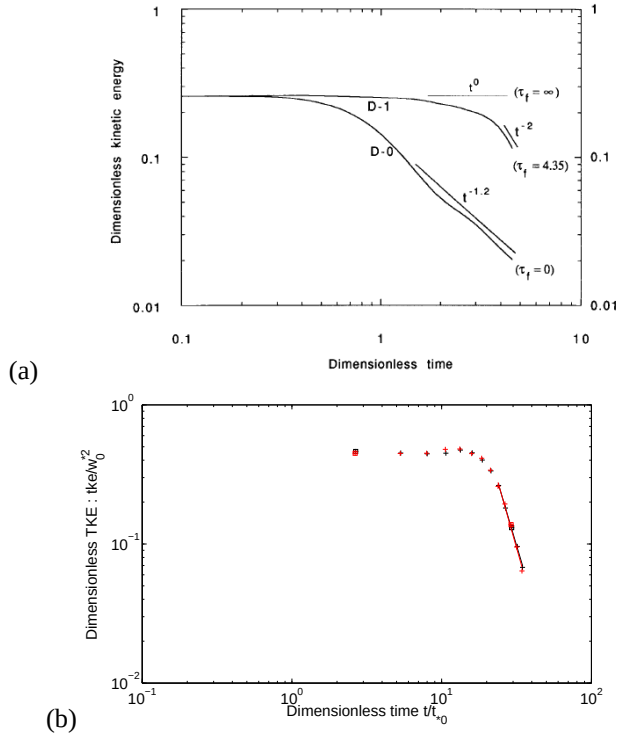

Figure 8: *The volume averaged total TKE, scaled by w_{*0}^2 as a function of the dimenionless time t/t_{*0}. (a) : according to Sorbjan and (b) with NCAR (black), Meso-NH (red) simulations*

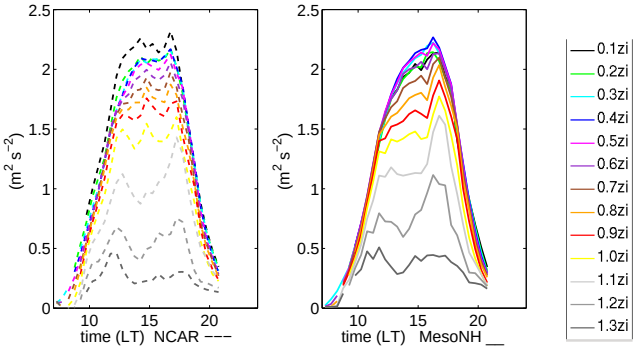

Figure 9: *Temporal evolution of the TKE at different heights in the ABL*

this is confirmed by the evolution of variances of the horizontal and vertical wind components (not shown here) : the increase of the TKE is due to a strong increase of the horizontal variances, whereas the vertical variance has a constant shape. This illustrates the importance of considering both the convective and the dynamical production when studying the TKE decay. Goulart et al. (2003) studied the role of the mechanical energy at surface on the TKE decay. The next step will be to also study the role of the wind shear at the top of the ABL. The decay of the TKE has been investigated at different heights in the ABL, for different surfaces and different synoptic conditions, during the BLLAST experiment, and the analysis is presented in Darbieu et al. (2012).

4. Conclusion

The results of two simulations (NCAR and Meso-NH) have been investigated, for a convective boundary layer case, without cloud, during the LAT. Overall, both simulations give similar results for mean parameters and fluxes.

All the convective boundary layer studies lean on Deardorff (1972) scalings (z_i, w_*, t_*, θ_*, q_*) whose definition and estimation during the LAT were investigated in this study. We showed that the estimation of the length scale z_i is very coherent whatever the method used during the convective development of the ABL. On the contrary, during the LAT, the most reliable method seems to be the determination of the mixed layer depth using a threshold on the near-zero vertical gradient of potential temperature. The other method leaning on the minimum value of the buoyancy flux should not be used because of the gradual loss of the universal shape of the vertical profile.

Besides, the diminishing w_* as well as the exponential increase of t_* from 1600 LT indicate that these normalization scales might not have still a meaning in the LAT. van Driel and Jonker (2011) suggest new normalization scales, by prognosing the TKE from a rate equation that comprised dissipation and buoyancy production.

We also have considered the evolution of the shape of buoyancy flux profiles. As in Sorbjan (1997) and Pino et al. (2004) works, the linear profiles of buoyancy fluxes are not maintained in the LAT and become ` S ´ shaped. We estimate the loss of linearity around 1700 LT.

As Sorbjan (1997), we found that the decay of the TKE is a function of two scales : the external time scale τ_f and the convective time scale t_{*0}. However, Sorbjan (1997) used the normalization scales w_{*0} and t_{*0} defined when the surface heat flux is maximum, that is to say when the ABL is fully convective. However, this law is not valid anymore when a time varying normalization scale is used. In the late afternoon, the limit of definition of these scales is reached.

To pursue the study of the TKE decay, we have evaluated the evolution of the TKE at different heights in the ABL : there might be a propagation of the TKE from the top to the middle of the ABL, in an anisotropic way : with the diminishing surface heat flux, dynamic processes, such as entrainment, gain the upper hand over thermal processes.

Finally, most of the parameters change abrutly between 1600 LT and 1700 LT, that is to say two hours after the maximum surface heat flux. Further study is needed to verify how much this is linked with the abrupt surface heat flux decrease at that time. Are these sharp changes linked with a longer time reaction of the ABL relative to the changes at surface ?

REFERENCES

Courant, K. L. H., R.; Friedrichs, 1967: On the partial difference equations of mathematical physics, *IBM Journal of Research and Development*, **2**, 215–234.

Couvreux, F., F. Guichard, J. L. Redelsperger, C. Kiemle, V. Masson, J. P. Lafore, and C. Flamant, 2005: Water-vapour variability within a convective boundary-layer assessed by large-eddy simulations and ihop-2002 observations, *Quart. J. Roy. Meteorol. Soc.*, **131**, 2665–2693.

Darbieu, C., F. Lohou, M. Lothon, D. Alexander, O. Decoster, S. Derrien, P. Durand, D. Legain, O. Traull, E. Pardyjak, H. Pietersen, and E. Pique, 2012: Turbulent kinetic energy decay in the late afternoon over heterogeneous surface: Bllast experiment, *20th Symposium on Boundary Layers and Turbulence*.

Deardorff, J. W., 1972: Parameterization of the planetary boundary layer for use in general circulation models, *Mon. Wea. Rev.*, **100**, 93–106.

Goulart, A., G. Degrazia, U. Rizza, and D. Anfossi, 2003: A theoretical model for the study of convective turbulence decay and comparison with Large-Eddy Simulation data, *Boundary-Layer Meteor.*, **107**, 143–155.

Lothon et al, ., 2012: The bllast field experiment : Boundary layer late afternoon and sunset turbulence., *Submitted to Bull. Amer. Met. Soc.*

Niewstadt, F. and R. Brost, 1986: The decay of convective turbulence., *Journal of the Atmospheric Sciences*, **42**, 532–546.

Pino, D., H. J. J. Jonker, and J. Vilà-Guerau de Arellano, 2004: Role of the shear and inversion strength during sunset turbulence over land: characteristic length scales, *In: Proc: 16th AMS Symposium on boundary layers and turbulence, 9-13 August 2004, Portland, Maine, American Meteorological Society, 45 Beacon ST., Boston, MA*.

Sorbjan, Z., 1997: Decay of convective turbulence revisited, *Boundary-Layer Meteorol.*, **82**, 501–515.

—, 2007: A numerical study of daily transitions in the convective boundary layer, *Boundary-Layer Meteorol.*, **123**, 365–383.

van Driel, R. and H. J. J. Jonker, 2011: Convective boundary layers driven by non-stationary surface heat fluxes, *J. Atmos. Sci.*, **68**, 727–738.

Weckwerth, T., D. B. Parsons, S. E. Koch, J. A. Moore, B. B. Demoz, C. Flamant, B. Geers, J. Wang, and W. F. Feltz, 2004: An overview of the international H20 project (IHOP_2002) and some preliminary highlights, *Bull. Amer. Meteorol. Soc.*, **85**, 253–277.